Friction stir welding of Monel alloy at different heat input conditions

Heidarzadeh, Akbar; Chabok, Ali; Pei, Yutao

Published in:
Materials Letters

DOI:
10.1016/j.matlet.2019.02.108

Publication date:
2019

Materials Letters 245 (2019) 94–97

Contents lists available at ScienceDirect

Materials Letters

journal homepage: www.elsevier.com/locate/mlblue

Friction stir welding of Monel alloy at different heat input conditions: Microstructural mechanisms and tensile behavior

Akbar Heidarzadeh [a,*], Ali Chabok [b], Yutao Pei [b]

[a] Department of Materials Engineering, Azarbaijan Shahid Madani University, Tabriz, Iran
[b] Department of Advanced Production Engineering, Engineering and Technology Institute Groningen, University of Groningen, Nijenborgh 4, 9747 AG Groningen, The Netherlands

ARTICLE INFO

Article history:
Received 7 December 2018
Received in revised form 3 February 2019
Accepted 24 February 2019
Available online 27 February 2019

Keywords:
Monel
Welding
Microstructure
Mechanical properties

ABSTRACT

The mechanisms governing the microstructural evolution during friction stir welding of Monel at different heat inputs and the corresponding mechanical properties were investigated. In the low heat input condition, both continuous and discontinuous dynamic recrystallizations caused the formation of fine grains with an average grain size of 1.7 μm and closely random texture. A high heat input condition resulted in larger average grain size of 23.5 μm with shear texture by only the continuous dynamic recrystallization. Low heat input led to the simultaneous increase of strength and elongation. The origins of the tensile behavior of the joints have been discussed.

1. Introduction

Friction stir welding (FSW) is a promising joining method, which eliminates the issues of fusion welding [1]. Many researches have shown that FSW can be used to weld different metals and alloys [2]. However, an investigation into the FSW of Monel alloys is lacking. For the first step of the Monel FSW, it is very necessary to have an understanding about the microstructural evolution during the process. On the other hand, it is reported that the heat input amount can influence the mechanism of the grain structure formation during FSW [3]. Therefore, in this study, it has been tried to investigate the microstructure evolution during FSW of Monel at both low and high heat input conditions. It is expected that the outcomes of the current study would open a new window for joining Monel alloys.

2. Materials and methods

2 mm thick Monel 400 plates were friction stir welded at different heat inputs. For the low and high heat input conditions, the tool rotational and traverse speeds were, respectively, 450 rpm/100 mm min^{-1} and 900 rpm/25 mm min^{-1}. A WC-Co tool consisted of a ø12 mm shoulder and a pin of ø3 × 1.75 mm was employed. The peak temperature was measured during FSW using K type thermocouples inserted into the back side of the plate. The microstructure of the joints were characterized using orientation imaging microscopy (OIM) with a step size of 70 nm at different microstructural zones. For studying the tensile properties, specimens were prepared according to ASTM-E8 M standard, and then the tensile tests were carried out at a strain rate of 1 mm min^{-1}.

3. Results and discussion

The OIM results of the BM, including inverse pole figure (IPF) map, misorientation angle distribution (MAD), and pole figures (PFs) are illustrated in Fig. 1. From Fig. 1a and b, the BM is composed of large equiaxed grains with an average grain size of 17.4 μm. The grain boundaries (GBs) are composed of 62.8% high angle grain boundaries (HAGBs), 10.9% low angle grain boundaries (LAGBs), and 26.3% twin boundaries (∑3 TBs). The BM has a nearly random texture with a maximum strength of 1.4.

Fig. 2 shows the OIM of the transition from BM to stir zone (SZ) of the low heat input joint. From Fig. 2a, no heat affected zone (HAZ). In the thermomechanically affected zone (TMAZ) close to the BM (Fig. 2b), the initial TBs are transforming to the HAGBs shown by white ellipses. This is why the amount of TBs decreases in the TMAZ down to 13.8% (Fig. 2h). The bulging of the original GBs along with the formation of LAGBs is observed as indicated by white arrows (Fig. 2b). In some areas (for instance indicated by a green arrow in Fig. 2b), the bulged boundaries have become a new recrystallized nucleus by the formation of TBs behind them, which is a clear sign of discontinuous dynamic recrystallization (DDRX) mechanism. Thus, in Fig. 2h, the origin of 32.2% TBs in

* Corresponding author.
E-mail address: ac.heydarzadeh@azaruniv.ac.ir (A. Heidarzadeh).

https://doi.org/10.1016/j.matlet.2019.02.108
0167-577X/

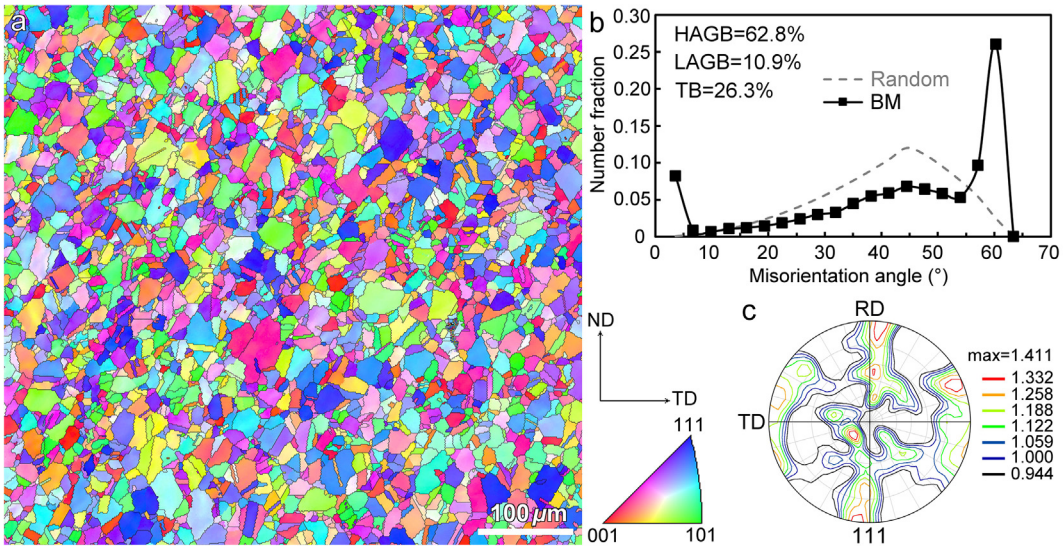

Fig. 1. Orientation imaging microscopy of the BM: (a) IPF map, (b) Misorientation angle distribution in conjunction with grain boundary characterization distribution and (c) (1 1 1) PF.

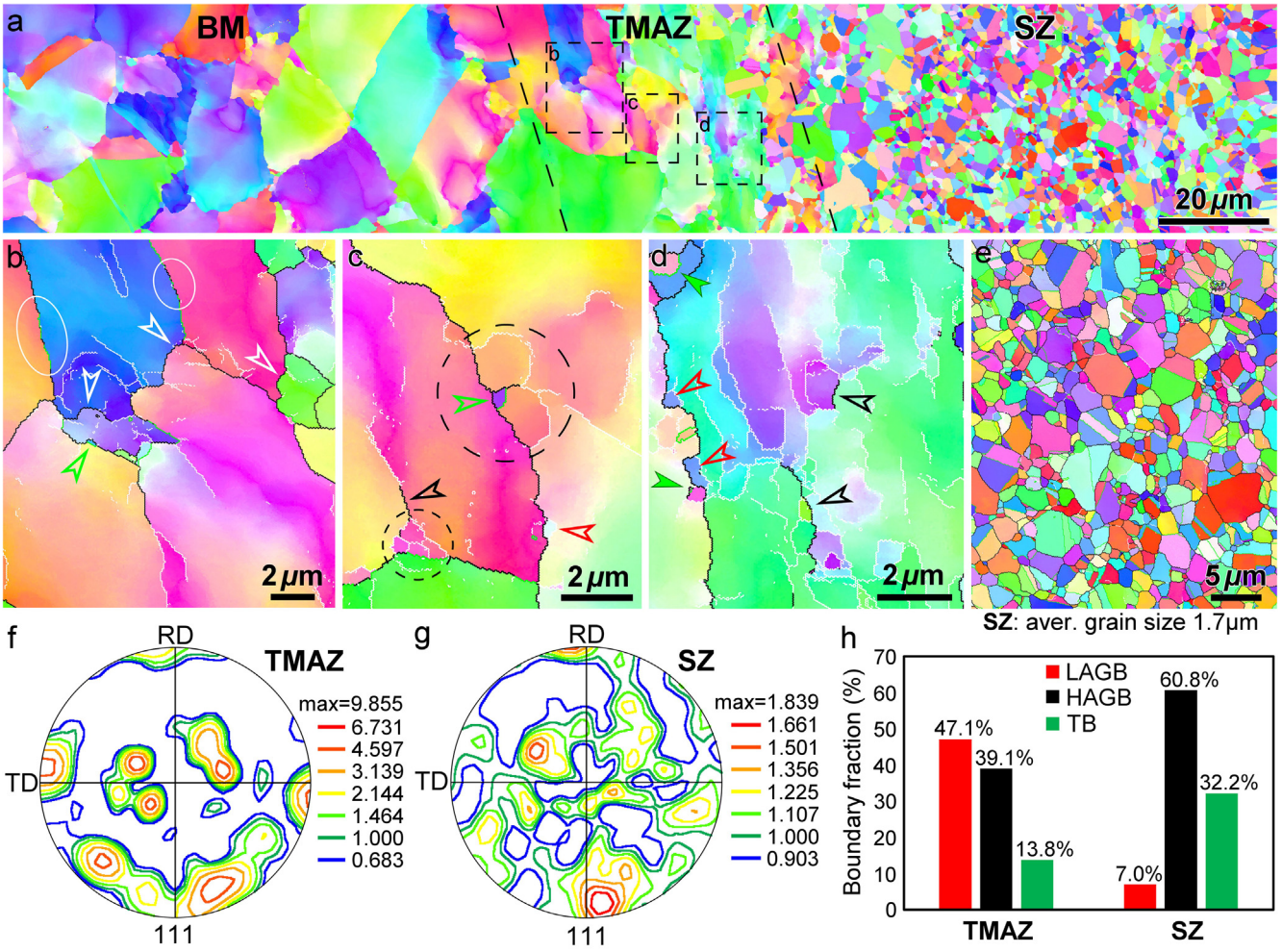

Fig. 2. (a) Overall IPF map of the low heat input joint (advancing side); (b, c and d) IPF + GB maps of the TMAZ at higher magnification of three areas indicated by rectangles in (a), respectively. The HAGBs, LAGBs, and the TBs are marked by black, white, and green colors, correspondingly. The white, green, red and black arrows point to the bulged GBs, formed TBs at bulged GBs, bulged TBs and formed LAGBs, and partly transformed LAGBs to HAGBs. The dashed white and black circles show the transformation of initial TBs to random HAGBs, and the formation of subgrains nearby the GBs, respectively. (e) IPF + GB maps of the SZ. (f, g) (1 1 1) PFs of the TMAZ and SZ respectively. (h) GBCD of the TMAZ and SZ. (For interpretation of the references to colour in this figure legend, the reader is referred to the web version of this article.)

the SZ can be divided into two mechanisms: formation of TBs during DDRX and growth of DRX grains.

In the next area, i.e. Fig. 2c, the other type of DDRX mechanism was detected as marked by a red arrow. In this type of DDRX, the formation of LAGBs instead of TBs behind the bulged GBs results in new nuclei. In conjunction with DDRX, in some areas, especially near to the old GBs and triple points (indicated by dashed black circles and black arrow in Fig. 2c), formation of new subgrains and transformation of LAGBs to HAGBs have occurred. This mechanism causes that, from the BM to the TMAZ, the amount of LAGBs increases from 10.9% to 47.1%, and then decreases to 7.0% in the SZ (Fig. 2h). This means that dynamic recovery (DRV) and continuous dynamic recrystallization (CDRX) are the other mechanisms governing the gain structure formation in this region.

Fig. 2d shows that the amount of CDRX increases as approaching the SZ. This effect can be explained by the so-called Zener-Holloman parameter (Z) [4]. As approaching the SZ, the strain and strain rate increase, which means higher Z values. At higher Z values, grain boundary sliding (GBS) and hence the GB bulging are inhibited [5]. In addition, CDRX needs higher amounts of strains [6,7].

Fig. 2e shows that the final microstructure in SZ consisting of equiaxed grains with an average size of 1.7 μm. The (1 1 1) IPFs of the TMAZ and the SZ (Fig. 2f and g) reveal that the shear texture (with a maximum intensity of 9.85) becomes more random in the SZ (with a maximum intensity of 1.84). The origin of the texture strength reduction in the SZ made at the low heat input condition is DDRX.

Fig. 3 illustrates the OIM result of the transition region of the high heat input joint. From Fig. 3a, the high heat input joint included a wider TMAZ. In addition, a wide HAZ was formed with larger grain size and more TBs than in the BM (Fig. 3a-b). In the TMAZ (Fig. 3c), only CDRX (indicated by black arrows) was detected. The increment of LAGBs from the BM to the TMAZ (from 10.8% to 55.8%) and then the decrease of them in SZ to 19.2% are the other sign of CDRX. According to Fig. 3d, the SZ contains large grains with an average size of 23.5 μm. The peak temperature was measured as 949 K and 1218 K, respectively, for the low and high heat input FSW. The strain rate and Z value were estimated to be 23.5 s^{-1}/48.0 × 10^6 s^{-1} and 108.3 s^{-1}/8.9 × 10^6 s^{-1} for the low and high heat input FSW, respectively, according to the model of flow stresses during hot deformation of metals [8,9]. Thus, the Z value was about 5 times higher and the peak temperature was lowered about 270 K in the case of the low heat input joint, and hence the grain size was much refined with limited grain growth at lower temperatures. The texture results show that the grain growth caused higher texture strength of 3.79 (Fig. 3e) in the HAZ. Furthermore, the grains of the SZ with a maximum texture strength of 7.83

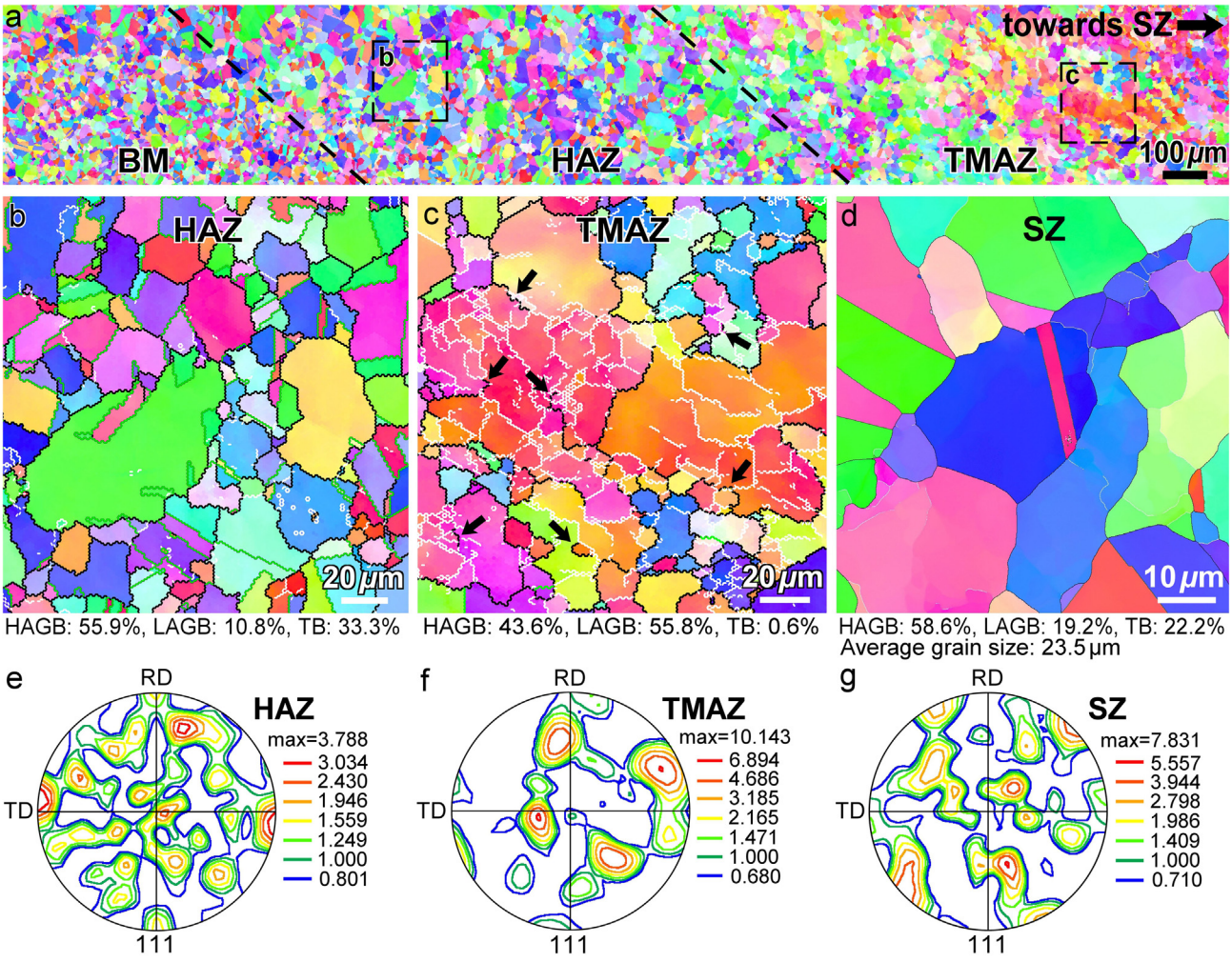

Fig. 3. (a) Overall IPF map of the high heat input joint (advancing side); (b, c) High magnification IPF + GB map of the HAZ and TMAZ, respectively, of the areas indicated by rectangles in (a) with the HAGBs, LAGBs and the TBs marked by black, white and green colors, correspondingly. The black arrows indicate the partly transformed LAGBs to HAGBs. (d) High magnification IPF + GB map of the SZ; (e, f and g) (1 1 1) PFs of the HAZ, TMAZ and SZ, respectively. (For interpretation of the references to colour in this figure legend, the reader is referred to the web version of this article.)

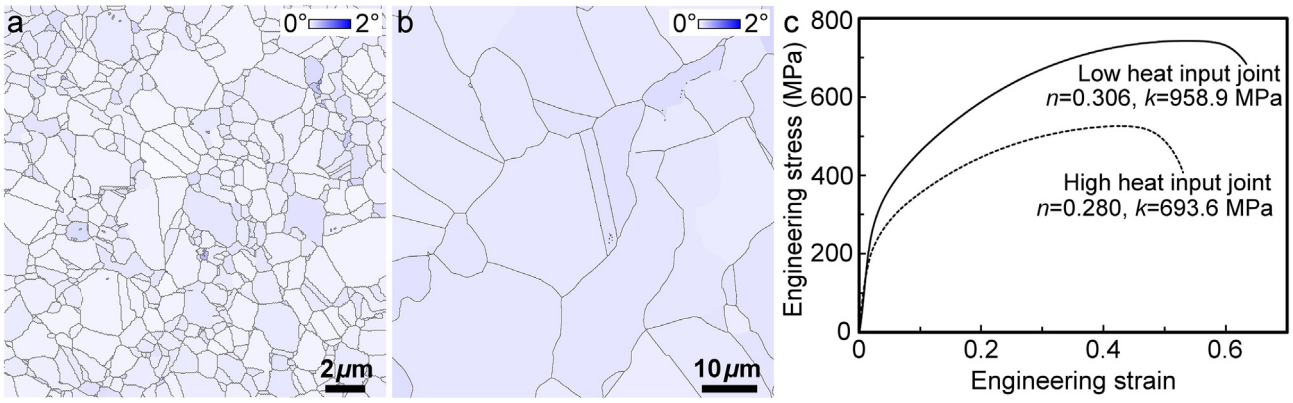

Fig. 4. GAM maps of the SZs made at (a) low heat input and (b) high heat input; (c) engineering stress-strain curve of the two types of joints with n and k being the strain hardening exponent and strength coefficient, respectively.

(Fig. 3g) have inherited at a large extent from the shear texture as observed in the TMAZ with maximum strength of 10.14 (Fig. 3f), which confirms that the only mechanism is CDRX.

Tensile engineering stress-strain curves together with the grain average misorientation (GAM) maps of the SZs are illustrated in Fig. 4. According to Fig. 4a and b, the SZs made at the low and high heat input respectively have not a considerable difference in dislocation densities. From Fig. 4c, the low heat input joint exhibits a simultaneous increase of both the strength and elongation. The strain hardening exponent (n) and strength coefficient (k) were calculated as 0.306 and 958.9 MPa, and 0.280 and 693.6 MPa for the low and high heat input joints, respectively. Much finer grain sizes, more HAGBs (93% versus 80.8% in the high heat input SZ) and more random texture of the low heat input SZ lead to larger elongation together with higher strain hardening capacity (n).

4. Conclusions

The heat input amount has an extensive effect on the microstructure evolution during FSW and the mechanical properties of the Monel. At low heat input condition, DDRX and CDRX result in the formation of fine grains with a large amount of HAGBs and a nearly random texture. At high heat input condition, CDRX causes large grown grains with a shear texture. The low heat input condition results in synergic increase of the strength and elongation. Finer grain size, larger Taylor factor, more HAGBs and random texture of the SZ are the main reasons of the better tensile behavior of the low heat input joint.

Conflict of interest

The authors declare that there is no conflict of interest regarding the publication of this article.

References

[1] G. Çam, Int. Mater. Rev. 56 (2011) 1.
[2] S. Mironov, T. Onuma, Y.S. Sato, H. Kokawa, Acta Mater. 100 (2015) 301.
[3] S. Mironov, K. Inagaki, Y.S. Sato, H. Kokawa, Philos. Mag. 95 (2015) 367.
[4] C. Zener, J.H. Hollomon, J. Appl. Phys. 15 (1944) 22.
[5] T. Sakai, A. Belyakov, R. Kaibyshev, H. Miura, J.J. Jonas, Prog. Mater. Sci. 60 (2014) 130.
[6] F.J. Humphreys, M. Hatherly, Recrystallization and Related Annealing Phenomena, second ed., Elsevier, Oxford, 2004.
[7] T.R. McNelley, S. Swaminathan, J.Q. Su, Scripta Mater. 58 (2008) 349.
[8] C.I. Chang, C.J. Lee, J.C. Huang, Scripta Mater. 51 (2004) 509.
[9] A. Laasraoui, J.J. Jonas, Metall Trans A 22 (1991) 1545.